Behavior of Geotextile-Reinforced Clay with a Coarse Material Sandwich Technique under Unconsolidated-Undrained Triaxial Compression

Kuo-Hsin Yang[1]; Wubete Mengist Yalew[2]; and Minh Duc Nguyen[3]

Abstract: This paper presents a series of unconsolidated-undrained (UU) triaxial compression tests for investigating the behavior and failure mechanism of geotextile-reinforced clay and the effects of sandwiching nonwoven geotextile in a thin layer of sand (sandwich technique) on improving the shear strength of reinforced clay. Test variables include confining pressures, the number of geotextile layers, and thicknesses of the sand layers. The mobilized tensile strain of reinforcements, estimated according to the residual tensile strain by using a digital image–processing technique, was used to directly quantify the effects of soil-geotextile interaction on the shear-strength improvement. The test results showed that the shear strength of reinforced clay increased as the number of geotextile layers was increased. Failure patterns were changed from classical Rankine-type failures for unreinforced soil specimens to bulging (barrel-shaped) failures between adjacent geotextile layers. The effectiveness of reinforcing clay by applying nonwoven geotextile can be attributed to an increase in the apparent cohesion of the reinforced clay specimen. Regarding the sandwich technique, the test results revealed that layers of sand encapsulating the reinforcement can effectively provide an improved soil-geotextile interaction, thereby enhancing the shear behavior of reinforced clay. The shear strength increased as the thickness of the sand layer was increased. An optimal value of sand-layer thickness for maximum shear-strength improvement was not observed at large confining pressures. An appreciable shear-strength improvement was still observed when the sand-layer thickness was increased from 15 to 20 mm at $\sigma_3 > 100$ kPa. The sandwich technique contributes to shear-strength improvement by increasing the friction angle of reinforced specimens. The mobilized tensile strain and force of the geotextile increased as the number of geotextile layers, thicknesses of the sand layers, and confining pressure were increased. The mobilized tensile strain and force were strongly correlated to the strength difference between reinforced and unreinforced soil. This experimental finding demonstrated that mobilized tensile strain and force directly contribute to the shear-strength improvement of reinforced clay. **DOI: 10.1061/(ASCE)GM.1943-5622.0000611.**

Author keywords: Geotextile-reinforced clay; Coarse material; Sandwich technique; Mobilized tensile strain; Triaxial test.

Introduction

Geosynthetic-reinforced soil (GRS) structures, in which geosynthetic reinforcements are embedded in a soil mass, have several distinct advantages over conventional retaining structures because of their ductility, high tolerance to differential settlement without structural distress, rapid method for construction, cost effectiveness, and adaptation to different site conditions. The backfill material forms one of the major constituents of GRS walls and slopes and accounts for 30–40% of their cost. For effective performance of reinforced earth structures, current design guidelines (Elias et al. 2001; AASHTO 2002; Berg et al. 2009; NCMA 2010) conventionally specify using free-draining granular materials as backfill materials within a reinforced zone and preclude the use of fine-grained materials (Fig. 1). The *compliant* soils shown in Fig. 1 are backfills that comply with the criteria of either design guidelines, whereas the *marginal* soils are those that do not. In addition to the gradation limits, the plasticity index (PI) of the backfill is also specified (PI ≤ 6 for walls and 20 for slopes). Because marginal backfills typically have low permeability, they are referred to by terms such as poorly draining, low-permeability, low-quality, cohesive, and fine-grained backfills.

To reduce the construction cost of GRS structures and minimize the transportation cost and environmental impact associated with the disposal of the excavated soil, locally available marginal soils have been used as alternative backfills. The main concern with using marginal soils as backfill is the possibility of a buildup of positive-pore water pressure either during construction or after a rainfall event, which may weaken the soil, resulting in a reduction in the soil shear strength and soil-reinforcement interface strength. The inherent low strength, moisture instability, possible volume changes, and creep potential are other concerns with using marginal backfill (Zornberg and Mitchell 1994). However, with the accumulated experience and knowledge in both the construction and research of GRS structures with marginal backfills (Glendinning et al. 2005; Chen and Yu 2011; Taechakumthorn and Rowe 2012), these concerns can be appropriately alleviated by adopting suitable construction techniques and drainage systems.

Drained and undrained triaxial compression tests on reinforced clay and silt, representative of soil elements inside GRS structures, have been conducted to analyze the shear behavior of reinforced

[1]Associate Professor, Dept. of Civil and Construction Engineering, National Taiwan Univ. of Science and Technology, 43, Sec. 4, Keelung Rd., Taipei 106, Taiwan (corresponding author). E-mail: khy@mail.ntust.edu.tw

[2]Lecturer, Faculty of Civil and Water Resources Engineering, Bahir Dar Univ., P.O. Box 26, Bahir Dar, Ethiopia. E-mail: wubmngst@gmail.com

[3]Lecturer, Dept. of Soil Mechanics and Foundations, Univ. of Technology and Education, Ho Chi Minh City, Vietnam. E-mail: ducnm@hcmute.edu.vn

Note. This manuscript was submitted on March 17, 2015; approved on September 2, 2015; published online on December 16, 2015. Discussion period open until May 16, 2016; separate discussions must be submitted for individual papers. This paper is part of the ***International Journal of Geomechanics***, © ASCE, ISSN 1532-3641.

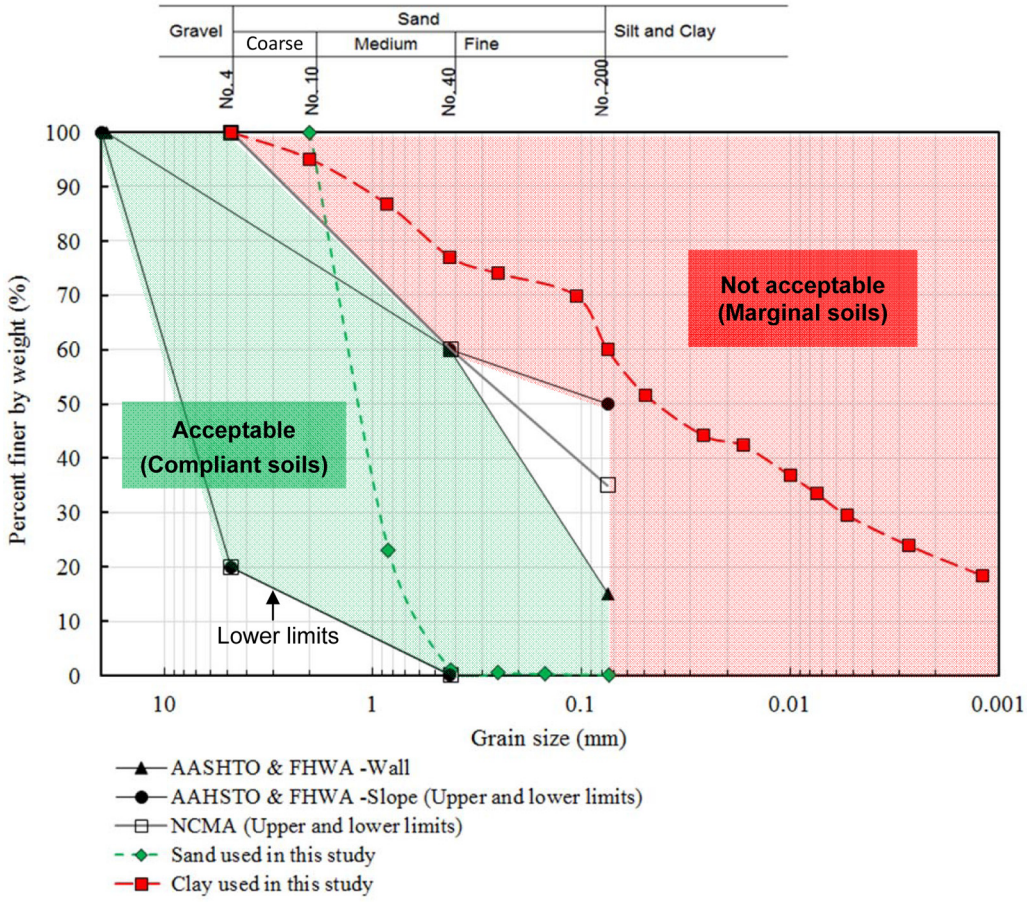

Fig. 1. Grain-size distribution of backfill in GRS structures as recommended by design guidelines and the soils used in this study

marginal soils (Ingold 1983; Ingold and Miller 1982, 1983; Fabian and Fourie 1986; Fourie and Fabian 1987; Al-Omari et al. 1989; Indraratna et al. 1991; Noorzad and Mirmoradi 2010; Jamei et al. 2013). Ingold and Miller (1982) found that permeable reinforcements can enhance the shear strength of the reinforced clay because the excess pore water pressure generated during undrained loadings can dissipate through radial migration from the soil into the reinforcements. However, for clay reinforced with impermeable reinforcements, the undrained shear strength decreased substantially less than that of an unreinforced sample. The Skempton pore water pressure parameter (A) was applied to explain this phenomenon. Since impermeable reinforcement did not allow drainage, high excess pore water pressure developed and accumulated at the clay-reinforcement interface, which resulted in premature failure along the interface and finally led to the failure of the specimen. Fabian and Fourie (1986) reported that high-permeable reinforcements could increase the undrained shear strength of reinforced silty clay by nearly 40%, whereas low-permeable reinforcements can decrease the undrained strength by a similar amount. Al-Omari et al. (1989) found that progressively developed slippage at the clay-geomesh interface caused the failure mode of overconsolidated geomesh-reinforced clay. The reinforcing effect in the undrained condition is a result of an increase in cohesion, whereas in the drained condition, the effect is a result of an increase in friction angle. Noorzad and Mirmoradi (2010) found that the shear strength of the reinforced specimens was affected by the soil PI and compaction conditions (i.e., moisture content and relative compaction). Readers may also refer to Zornberg and Mitchell (1994) and Mitchell (1995) for a comprehensive review of experimental studies and case histories on evaluating the soil-reinforcement interaction mechanism.

The provision of thin layers of sand sandwiching on both sides of the reinforcement within clay soil (known as the sandwich or sand cushion technique) and its influence on improving the strength and deformation characteristics of reinforced clay have been investigated using direct shear tests (Abdi et al. 2009), pullout tests (Sridharan et al. 1991; Abdi and Arjomand 2011; Abdi and Zandieh 2014), and triaxial compression tests (Unnikrishnan et al. 2002). Experimental results demonstrated that thin sand-layer inclusions could increase the interface interaction between the clay and reinforcement, resulting in improving the overall shear strength of the reinforced clay. The sand also acted as a lateral drainage layer to dissipate excess pore water pressure during shearing. In addition, previous studies (Unnikrishnan et al. 2002; Abdi et al. 2009; Abdi and Arjomand 2011; Abdi and Zandieh 2014) have indicated an optimal sand-layer thickness. Providing sand-layer thicknesses higher than the optimal thickness has not led to further improvement in system performance. The optimal sand thickness ranges from 8 to 15 mm in unconsolidated-undrained (UU) and direct shear tests, and can reach 8 cm in the large-scale pullout tests. Because the optimal sand thickness can vary with the types of soil and reinforcement for any specific project, Abdi and Zandieh (2014) suggested that the optimal thickness of sand layers can be considered the minimum thickness required for practical applications. In addition to its mechanical function, the sandwich technique has been demonstrated to increase a soil-geotextile or soil-geocomposite system's lateral drainage capacity, accelerate pore water pressure dissipation within reinforced soil (Raisinghani and Viswanadham

2010), and reduce the long-term clogging of nonwoven geotextile drains (Lin and Yang 2014).

Regarding reinforced clay, few studies have focused on the mobilization of reinforcement tensile strain and load within soil specimens, which is a direct evidence of soil-reinforcement interaction and is essential for understanding the relationships between soil-reinforcement interactions and the shear-strength enhancement of reinforced clay. Accordingly, this study conducted a series of UU triaxial compression tests on nonwoven geotextile-reinforced clay to evaluate the effects of including nonwoven geotextile reinforcements and of using the sandwich technique. A digital image–processing technique proposed by Nguyen et al. (2013) was adopted for determining the residual tensile strain of reinforcements after tests and for estimating reinforcement tensile loads. The main objective of this study was to investigate mobilization of reinforcement tensile strain and load within reinforced clay and their relationships with the mobilized shear strength of reinforced clay. The study results provide useful information for effectively and appropriately applying the sandwich technique to GRS structures.

Experimental Program

A total of 32 UU triaxial compression tests were conducted to evaluate the effects of including nonwoven geotextile and thin sand layers on the mechanical behavior of clay. The undrained test conditions were selected to simulate the behavior of cohesive soils subjected to quick loadings (relative to the time required for the dissipation of pore water pressure of cohesive soils) after construction. The test variables were confining pressure, the number of geotextile layers, and thicknesses of the sand layers sandwiching the reinforcements. A digital image–processing technique was used to determine the deformation of reinforcement layers after triaxial tests.

Test Materials

Soils

Maokong clay and uniform quartz sand were used in this study. Fig. 1 shows the grain-size distribution of tested soil based on ASTM D422 (2007). The properties of clay and sand are summarized in Tables 1 and 2. The Maokong clay is obtained from the southeast mountain region of Taipei, Taiwan. This clay is classified as low-plasticity clay (CL) by the Unified Soil Classification System with specific gravity (G_s) of 2.72, liquid limit (LL) of 42, plastic limit (PL) of 21, and PI of 21. The optimum moisture content and maximum dry unit weight determined from standard proctor compaction (ASTM D698 2012) are ω_{opt} = 22.7% and $\gamma_{d,max}$ = 15.7 kN/m^3, respectively, and the corresponding degree of saturation calculated on the basis of the weight-volume relationship is nearly 90%. The undrained shear strength parameters obtained from UU tests (ASTM D2850 2007a) are cohesion (c_u = 84.7 kPa) and friction angle (ϕ_u = 13.1). The saturated hydraulic conductivity estimated using Terzaghi's one-dimensional consolidation theory is k_{sat} = 1.3 - $\times 10^{-10}$ m/s.

Table 1. Properties of Maokong Clay

Property	Value
Unified Soil Classification System	CL
LL (%)	42
PL (%)	21
PI (%)	21
Specific gravity (G_s)	2.72
Optimum moisture content (ω_{opt}; %)	22.7
Maximum dry unit weight ($\gamma_{d,max}$; kN/m^3)	15.7
Cohesion (c_u; kPa)	84.7
Friction angle (ϕ_u; degrees)	13.1
Saturated hydraulic conductivity (k_{sat}; m/s)	1.3×10^{-10}

The sand is uniform and clean quartz sand, classified as poorly graded sand (SP) by the Unified Soil Classification System. The specific gravity (G_s) coefficient of uniformity (C_u), and gradation (C_c) were 2.65, 2.17, and 1.04, respectively. The minimum and maximum dry unit weights of sand were $\gamma_{d,min}$ =14 kN/m^3 and $\gamma_{d,max}$ =16 kN/m^3. The sand layers were prepared carefully to maintain a target relative density of 70%. At this target density, the effective shear-strength parameters were obtained from triaxial compression tests as c' = 0 and ϕ' = 38.5°, and from direct shear test as c' = 0 and ϕ' = 38.8°. The sand-geotextile interface friction angle was ϕ_a' = 35.8°, within the normal stress range of 20–100 kPa, measured by a modified direct shear test (the top shear box was filled with soil, and steel platen was placed in the lower one). The saturated hydraulic conductivity from the constant head test was k_{sat} = 1.35×10^{-3} m/s.

Geotextile

A commercially available nonwoven fabric was used in this work. This material was selected on the basis of its large plastic deformation, such that residual deformation of the reinforcement can be preserved easily when the tensile force applied to the reinforcement was released after each test. The load-elongation behaviors of the reinforcement were tested by wide-width (ASTM D4595 2011) and biaxial tensile tests (Nguyen et al. 2013) in the longitudinal and transverse directions, and puncture-strength test (ASTM D6241 2009).

The puncture-strength test was used to evaluate the axisymmetric tensile behavior of geotextile associated with the geotextile samples in the reinforced specimens subjected to the axisymmetric loading conditions under triaxial tests. The puncture-strength test was performed using a modified California Bearing Ratio (CBR) steel mold with an inside diameter of 150 mm and a pair of collar clamps attached to the mold (Fig. 2). Abrasive papers were applied to the inner surfaces of collar clamps to prevent geotextile slippage during tests. A steel rod 50 mm in diameter was attached to a load ring and pushed the geotextile specimen downward at a constant rate of displacement. During the test, the test data recorded the vertical displacement (y) and the applied force of the puncture rod (P) and can be converted in the form of tensile load versus strain, representing the tensile load-strain response of geotextiles under axisymmetric conditions, by the following

Table 2. Properties of Quartz Sand

Property	Value
Unified Soil Classification System	SP
Specific gravity (G_s)	2.65
D_{10} (mm)	0.6
D_{30} (mm)	0.9
D_{60} (mm)	1.3
Coefficient of curvature (C_c)	1.04
Coefficient of uniformity (C_u)	2.17
Minimum dry unit weight ($\gamma_{d,min}$; kN/m^3)	14
Maximum dry unit weight ($\gamma_{d,max}$; kN/m^3)	16
Unit weight (γ; kN/m^3)	15.4
Cohesion (c'; kPa)	0
Friction angle (ϕ'; degrees)	38.5
Saturated hydraulic conductivity (k_{sat}; m/s)	1.35×10^{-3}

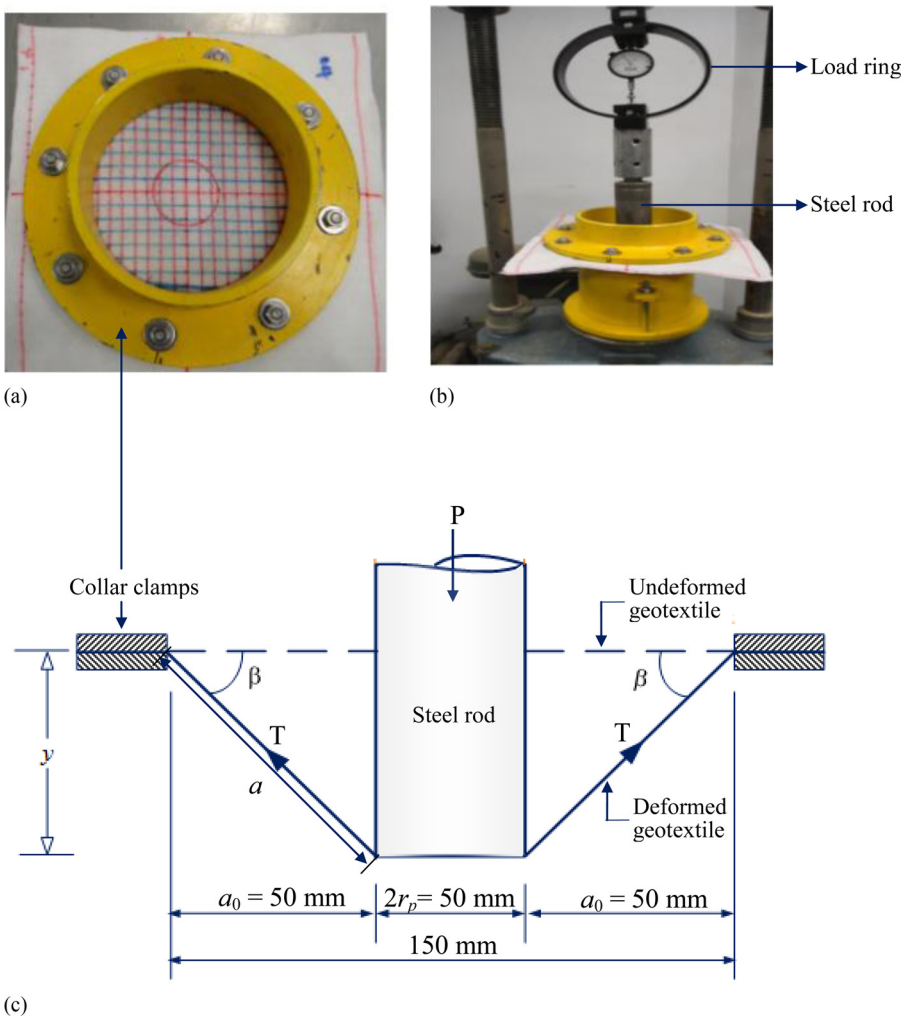

Fig. 2. Puncture-strength tests of geotextile: (a) geotextile clamped between collar clamps; (b) during test; (c) schematic of deformed geotextile and variables for calculating tensile strength

equations proposed by McGown et al. (1998) and Bergado et al. (2001). The tensile load in geotextile was calculated as follows:

$$T = \frac{P}{2\ \pi\ r_p \sin\beta} \tag{1}$$

where T = tensile force per unit width of geotextile in kN/m; P = measured puncture force in kN; r_p = radius of steel rod (25 mm); and β = angle between the deformed geotextile plane and initial horizontal position, as illustrated in Fig. 2. The value of β is obtained from the trigonometric function

$$\sin\beta = \frac{y}{a} = \frac{y}{\sqrt{y^2 + {a_0}^2}} \tag{2}$$

where y = vertical displacement of puncture rod; a_0 = initial length of geotextile from the inner edge of CBR mold to the outer edge of the steel rod; and a = deformed length of geotextile. The mobilized tensile strain (ε) is calculated according to the German standard [Deutsche Industrie Norm (DIN)]

$$\varepsilon = \frac{a - a_0}{a_0} \tag{3}$$

Fig. 3 shows the load-elongation responses of geotextile under wide-width and biaxial tensile tests and the puncture-strength tests. Tables 3 and 4 summarize the physical, hydraulic, and mechanical properties of geotextile. Based on permittivity test results (ASTM D4491 2007b), this geotextile is considered as a permeable reinforcement with a permeability of 3.5×10^{-3} m/s in the cross-plane direction, which is several orders of magnitude higher than the permeability of the clay used in this study. In addition, the tensile test results indicate that the geotextile is an anisotropic tensile material; the tensile strength and stiffness of the geotextile in the longitudinal direction (i.e., the stronger and stiffer direction) were larger than those in the transverse direction (i.e., the weaker and softer direction). Compared with various tensile test methods, the stiffness of geotextile obtained from biaxial tensile test, puncture-strength test, and wide-width tensile test ranges from small to large, respectively.

Specimen Preparation

A natural clay sample brought from a local site in the form of wet bulk was placed in an oven for a minimum of 24 h and then crushed and ground into dry powder in a mortar. Standard proctor compaction tests (ASTM D698 2012) were performed to determine the optimum moisture content and maximum dry density of the clay sample. Measured quantities of soil sample and water corresponding to

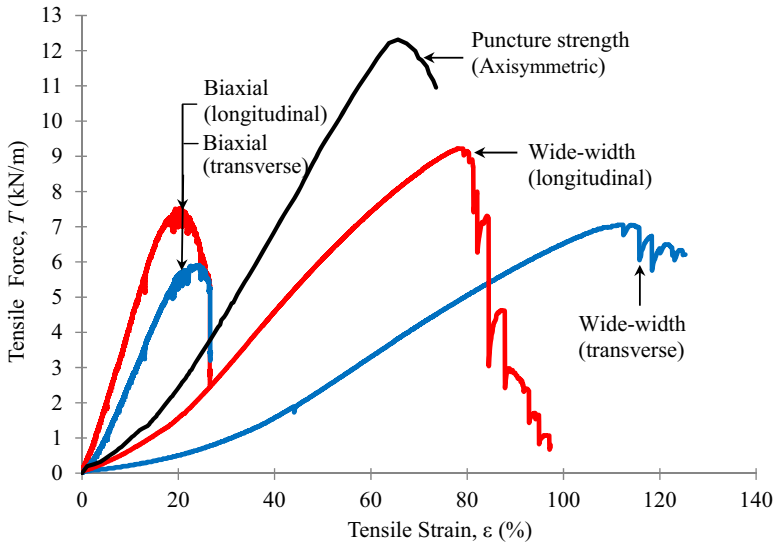

Fig. 3. Comparisons of tensile load-elongation response of nonwoven geotextile under various test conditions

Table 3. Physical and Hydraulic Properties of Nonwoven Geotextile

Property	Value
Fabrication process	Needle-punched polyethylene terephthalate nonwoven geotextile
Mass (g/m^2)	200
Thickness (mm)	1.78
Apparent opening size (mm)	0.11
Permittivity (s^{-1})	1.96
Cross-plane permeability (m/s)	3.5×10^{-3}

Table 4. Mechanical Properties of Nonwoven Geotextile

Direction	Ultimate strength (kN/m)	Failure strain (%)	Secant stiffness at peak value (kN/m)
Wide-width tensile test			
Longitudinal	9.28	84.1	11.03
Transverse	7.08	117.8	6.01
Biaxial tensile test			
Longitudinal	7.53	20.3	37.09
Transverse	5.91	24.3	24.32
Puncture strength test			
Axisymmetric	12.3	65.6	18.75

the optimum moisture content were mixed together, placed in a plastic bag within a temperature-controlled chamber, and sealed for a minimum of 2 days to ensure a uniform distribution of moisture within the soil mass.

A series of UU triaxial compression tests were performed on unreinforced clay, clay reinforced with the geotextile (reinforced clay specimen), and clay reinforced with the geotextile encapsulated in a thin layer of sand (sandwich specimen). A cylindrical soil specimen with a diameter of 50 mm and a height of 100 mm was prepared. For the unreinforced specimens, the clay was compacted in five layers by using a static compaction approach. For the reinforced clay specimens, the split mold was filled with clay in several layers, depending on the arrangement of the geotextile layers (Fig. 4). After each clay layer was compacted and leveled, the clay surface was scarified prior to adding the overlying geotextile layer and the next soil layer for developing favorable interface bonding with the overlying material. The reinforcement was then placed horizontally, and the amount of soil for the next layers was poured and compacted. This procedure was repeated until specimen preparation was completed. This specimen preparation procedure differs from those described by Ingold and Miller (1982) and Unnikrishnan et al. (2002). In their tests, the reinforced soil samples were prepared by cutting compacted clay samples by using a wire saw and trimming the cut faces, which did not model both the compacting of soil and the underlying reinforcement under actual construction conditions. The interface bonding in the sample prepared using the cutting method was likely less than that in the sample prepared using the proposed method of compacting the soil and geotextile together.

For the sandwich specimens (Fig. 5), clay was placed into a rubber membrane stretched inside a split mold. A vacuum pressure, between the mold and membrane, was applied to stretch the rubber membrane for easy preparation of the sample. After the clay was compacted and leveled to a desired height, half of the predetermined quantity of moist sand was placed and compacted with a small tamper to achieve the required thickness and density. The uniformity of thickness and density of the sand layer were carefully maintained over several trials. Afterward, the reinforcement layer was introduced above the lower part of the sand, and then the remaining portion of sand and clay soil was placed according to the aforementioned procedure.

Testing Program

A total of 16 tests were performed on the unreinforced and reinforced clay under different confining pressures (i.e., 50, 100, 150, and 200 kPa) and involving various numbers of geotextile layers (i.e., zero, one, two, and three layers). Regarding the reinforced clay constructed using the sandwich technique, a total of 16 tests were conducted by varying the thickness of the sand layer (i.e., 5, 10, 15, and 20 mm) and confining pressure (i.e., 50, 100, 150, and 200 kPa). The sand-layer thicknesses discussed in the remainder of the paper indicate the total thickness including the sand layers at the top and bottom of the nonwoven geotextile, as shown in Fig. 4(b). In UU tests, the specimens were not saturated (as compacted conditions) and were loaded axially at a strain rate of 1.5 mm/min. Because all of the reinforced specimens showed ductile behavior,

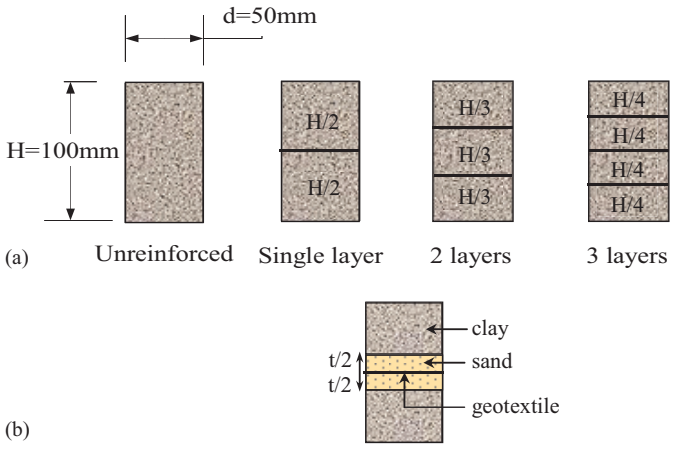

Fig. 4. Geotextile arrangements for triaxial compression tests on: (a) reinforced clay with various geotextile layers; (b) sandwich specimen

no definite peak was noticeable on the stress-strain curve. Thus, the tests continued until the strain levels of the reinforced specimens reached 20%, and this strain level was considered the failure strain. The same approach to selecting failure strains has been reported on by Ingold and Miller (1983), Fabian and Fourie (1986), and Unnikrishnan et al. (2002). Finally, the repeatability and consistency of the test results were carefully examined by conducting a few tests on the reinforced clay under the same conditions.

Technique for Measurement of Reinforcement Strain

The deformation of reinforcement under undrained loading was determined using a digital image–processing technique. The geotextile was cut into circular discs with a diameter of 50 mm, and the line along the diameter was divided into strips with a 10-mm line spacing marked by red and blue lines to indicate longitudinal and transverse directions, respectively. An image of the undeformed geotextile before tests was taken using a high-resolution digital camera [Fig. 6(a)]. After tests, the geotextile was retrieved from the reinforced specimen carefully, and the image (at the same resolution density) of the geotextile disc was taken immediately before further deformation occurred as a result of changes in the moisture distribution [Fig. 6(b)]. Then, the average residual tensile strain was calculated as

$$\varepsilon_r = \frac{d' - d}{d} \tag{4}$$

where ε_r = calculated residual tensile strain of a reinforcement; d' = diameter of the deformed geotextile specimen determined by counting the number of pixels (i.e., the fundamental unit of a digital image); and d = length of the undeformed reinforcement specimen in pixels.

Because the reinforcement was unloaded and retrieved from a dismantled specimen after each test, the measured residual tensile strain, representative of reinforcement plastic deformation, was less than its mobilized tensile strain during testing. In this study, residual and mobilized tensile strain relationships were established by first testing the reinforcement under various loading conditions at several target tensile strain levels, and then releasing the tensile loadings. Both target tensile strain values (controlled during tests) and the corresponding residual strain values (obtained after releasing the loading) were recorded and plotted. In Fig. 7, the mobilized and residual tensile strains appear to have a unique relationship, irrespective of different loading conditions. As a result, a linear function (i.e., $\varepsilon = 1.14\varepsilon_r + 4.16$) regressed from relationships between mobilized and residual tensile strain was constructed. The intercept in the linear function (as shown in Fig. 7) indicates that the plastic deformation of geotextile starts to occur when over 4% of the tensile strain is mobilized. This linear function is later used to determine the mobilized tensile strain from measured residual tensile strain.

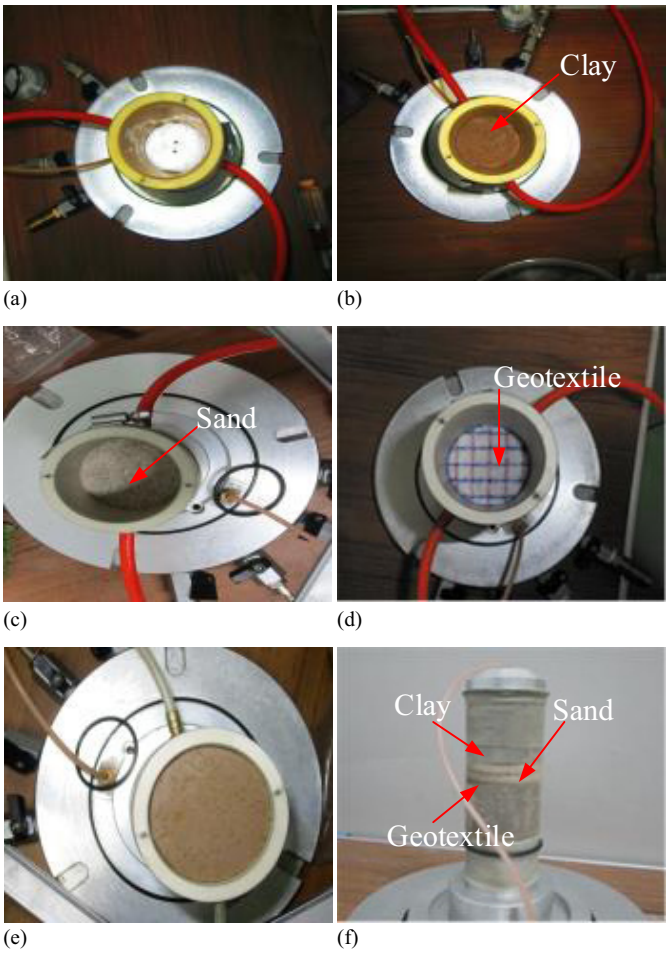

Fig. 5. Preparation of a reinforced clay specimen with the sandwich technique: (a) vacuum applied to stretch the membrane; (b) clay soil poured, compacted, and leveled; (c) half amount of sand placed; (d) geotextile placed horizontally; (e) top view of sandwich specimen inside the split mold; (f) completed sandwich specimen ready for test

Results and Discussion

Failure Pattern

Fig. 8 shows typical photos of deformed specimens after the tests. The unreinforced clay specimen [Fig. 8(a)] failed along a classic Rankine shear plane with an inclined angle of $45 + \phi'/2$. The reinforced clay specimens [Figs. 8(b–d)] had a ductile behavior that failed when bulging occurred between two adjacent reinforcement layers. No clear shear plane was observed in the reinforced clay specimens. As the number of geotextile layers was increased, the deformation became comparatively uniform (less bulging). This result suggests that including geotextile alters the failure pattern from brittle to ductile because of the flexibility of geotextile and the geotextile's capability of preventing the development of shear bands within a specimen. Similar failure patterns were reported by Fabian and Fourie (1986).

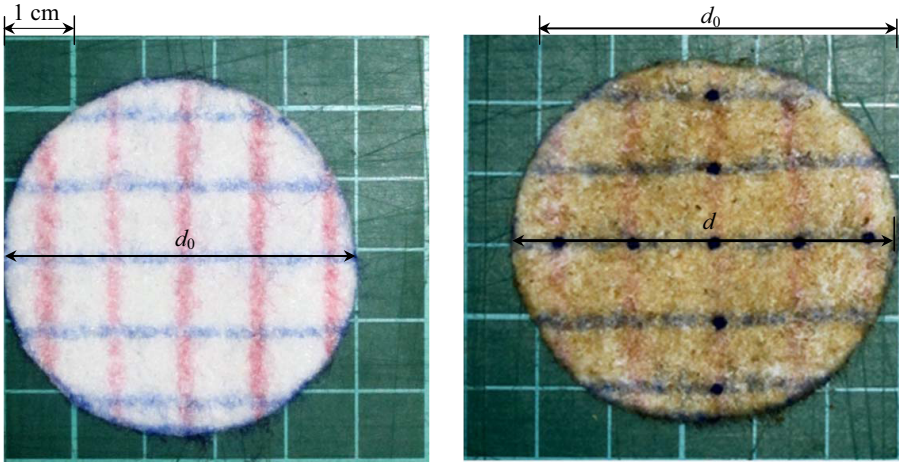

Fig. 6. Example of a geotextile specimen: (a) undeformed; (b) deformed after test

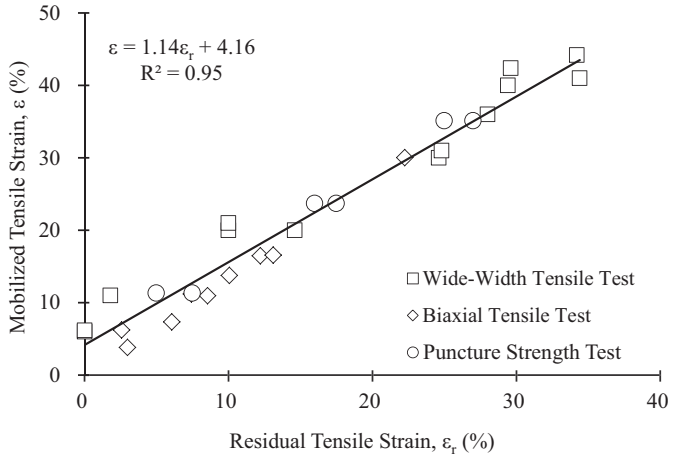

Fig. 7. Relationships between mobilized and residual tensile strains under various loading conditions

Fig. 8(e) presents a typical image of the deformed sandwich specimen. The failure was caused by a bulging of the clay and a discontinuous deformation at the sand-clay interface. The bulging and deformation were attributed to a lateral expansion of clay restrained by the sand-clay interface. Because the sand particles were prone to penetrate the clay [Fig. 8(f)], the sand-clay interface shear strength could be stronger than the shear strength of the clay itself. Thus, the zone of maximum lateral deformation moved away from the sand-geotextile interface to the clay.

After being tested, the geotextile was retrieved from the dismantled specimens, and the tensile deformation of the geotextile was closely analyzed. The tensile deformation was larger along the transverse direction (blue line in Fig. 6) than along the longitudinal direction (red line in Fig. 6) because the geotextile has higher stiffness in the longitudinal direction than in the transverse direction. Inspecting the geotextiles after the tests showed that no geotextile had broken at an axial strain of 20% by the completion of the test.

Stress-Strain Behavior

Fig. 9 shows the stress-strain responses of the unreinforced and reinforced clay specimens [Fig. 9(a)] and sandwich specimens [Fig. 9(b)] under a confining pressure of 200 kPa. Tables 5 and 6 present summaries of the test results regarding maximum deviatoric stress (i.e., $\sigma_{d,\ max}$) determined according to the measured stress-strain curves.

The reinforced clay specimens reached higher peak shear-strengths compared with the unreinforced soil specimens at a specific confining pressure, suggesting that including permeable reinforcements can effectively improve the undrained shear strength of clay. The peak shear strength increased as the number of geotextile layers and confining pressure were increased. This experimental result suggests that the clay-geotextile interaction is stronger under high confining pressure or narrow reinforcement spacing. The same observation has also been reported by Ingold and Miller (1982), Fabian and Fourie (1986), Indraratna et al. (1991), and Noorzad and Mirmoradi (2010). As explained by Noorzad and Mirmoradi (2010), the geotextile layers intercept the failure plane within the specimen, redistribute the mobilized stresses evenly within the soil, and hence enhance the shear strength of the reinforced soil.

At low strain levels (up to 3–5% of the axial strain), the unreinforced clay specimen exhibited a higher modulus (or mobilized higher shear strength) compared with the reinforced specimen [Fig. 9(a)]. The effects of reinforcement started (i.e., mobilized shear strength of the reinforced soil exceeded that of the unreinforced soil) under an axial strain ranging from approximately 3 to 5%. This result suggests that including a geotextile was not advantageous in enhancing the shear strength of the reinforced clay at a low strain level. The reinforcement requires a sufficient deformation to mobilize its tensile force for improving the overall shear strength of reinforced soil.

Regarding the sandwich specimens, the test results indicated that the shear strength of the sandwich specimen increased as the sand-layer thickness increased, and the efficiency of the sand thickness increased as the confining pressures increased [Fig. 9(b); Table 6]. This result suggests that providing a thin layer of sand around reinforcements is effective in enhancing the shear behavior of reinforced clay. Moreover, without the disadvantageous effect of reinforcement at a low strain level, the mobilized shear strength (or modulus) of the sandwich specimens at the low strain level significantly increased and could exceed that of the unreinforced clay for the sandwich specimens with thicker sand layers because the sand was stiffer than the geotextile. A practical implication of the research reported here is that the sandwich technique can be effective for reinforcement applications, such as pavements, in which the mobilized strain level is typically low.

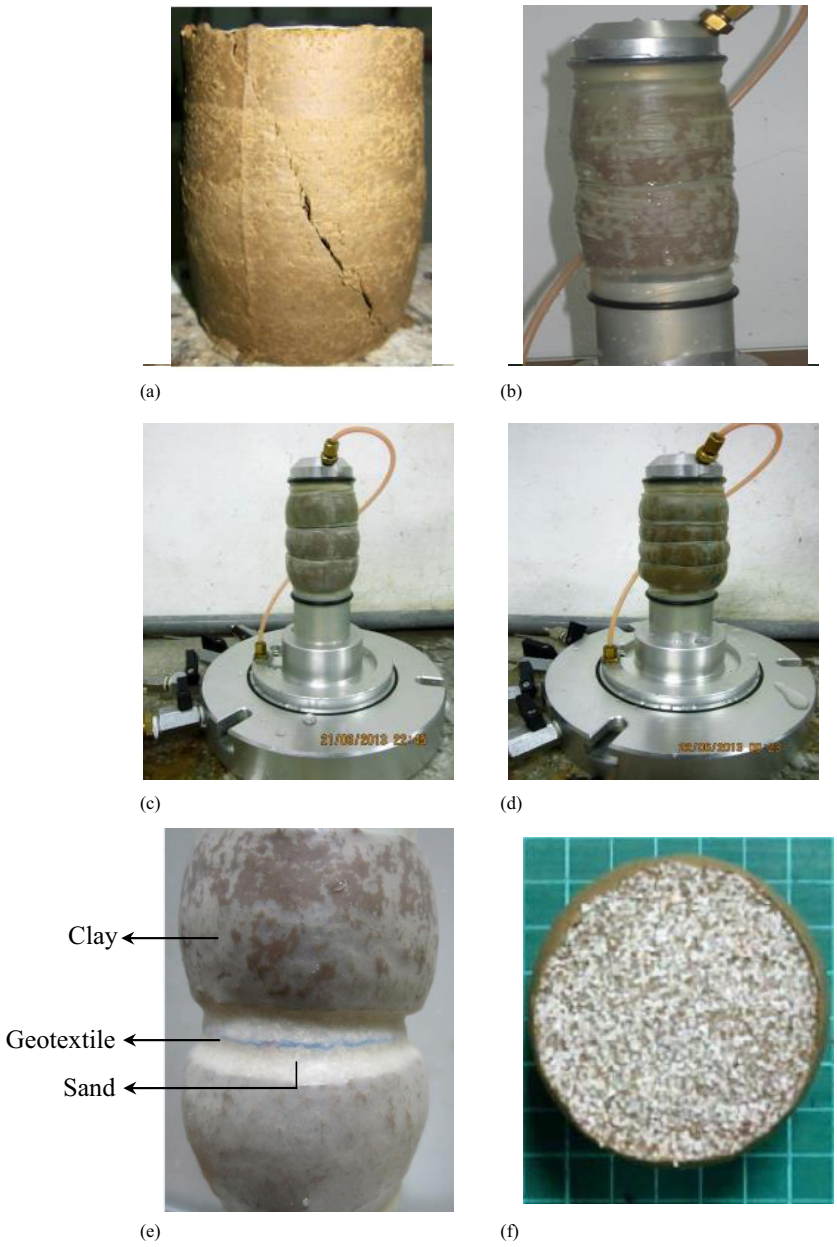

Fig. 8. Failure patterns of reinforced clay and sandwich specimens: (a) unreinforced; (b) single layer; (c) two layers; (d) three layers; (e) sandwich specimen; (f) sand-clay interface showing penetration of sand particles into clay (lower part of specimen)

Strength Improvement

The effects of including nonwoven geotextile and providing thin sand layers around reinforcements on shear-strength improvement were evaluated using the strength ratio and strength difference. The strength ratio (SR) is defined as the ratio of the maximum deviator stress of reinforced specimens to that of unreinforced specimens under the same confining pressure. The strength difference (SD) is defined as the shear-strength difference between reinforced specimens and unreinforced specimens at a specific confining pressure, which also indicates the net strength improvement from applying a reinforcement or sand layer

$$\mathrm{SR} = \frac{(\sigma_{d,\max})_{re}}{(\sigma_{d,\max})_{un}} \tag{5}$$

and

$$\mathrm{SD} = (\sigma_{d,\max})_{re} - (\sigma_{d,\max})_{un} \tag{6}$$

where $(\sigma_{d,\max})_{re}$ and $(\sigma_{d,\max})_{un}$ = maximum deviatoric stress of reinforced and unreinforced specimens, respectively.

Fig. 10(a) shows that the strength ratio of the reinforced clay increased as the reinforcement spacing decreased (i.e., as the number of geotextile layers increased). The results showed that the SR = 1.70–1.56 for specimens with a reinforcement spacing of 23.7 mm (i.e., three geotextile layers), whereas SR = 1.15–1.02 for specimens with a reinforcement spacing of 50 mm (i.e., a single geotextile layer). The shear-strength improvement was negligible (SR $\approx$ 1.0), especially for reinforced clay specimens with a single geotextile layer at $\sigma_3 \leq 100$ kPa. This result suggests that the weak clay-geotextile interaction existed under low confining pressure and large reinforcement spacing. Additionally, the effect of the confining pressure on the strength ratio is not clearly shown in Fig. 10(a). A

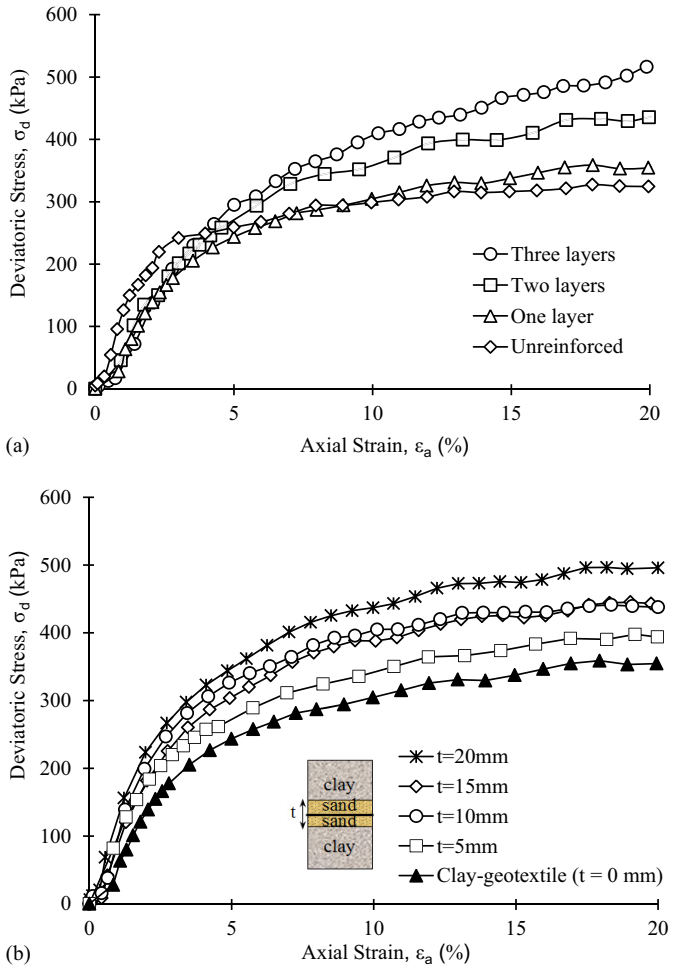

Fig. 9. Stress-strain response under undrained loading (σ_3 = 200 kPa): (a) reinforced clay specimens with different reinforcement layers; (b) sandwich specimen with different sand thicknesses

Table 5. Summary of UU Test Results of Reinforced Clay Specimens

Confining pressure (σ_3; kPa)	Maximum deviatoric stress ($\sigma_{d,max}$; kPa)			
	Unreinforced	One layer	Two layers	Three layers
50	236.4	246.7	349.5	401.9
100	278.7	285.0	399.2	436.4
150	304.6	347.6	405.6	476.9
200	324.3	358.7	435.5	517.3

possible explanation is that the soil undrained shear strength did not change much with the confining pressure during undrained tests. Similar conclusions can also be drawn from the strength difference data [Fig. 10(b)].

Fig. 11 shows that both the SR and SD of sandwich specimens increased as the sand-layer thickness increased. As discussed, a negligible shear-strength improvement was obtained for reinforced clay specimens with a single geotextile layer under low confining pressure; however, even with a minimal 5-mm sand cushion layer (2.5 mm on top and 2.5 mm on the bottom of the nonwoven geotextile), the SR is improved from SR = 1.04 to 1.20 at σ_3 = 50 kPa, and from SR = 1.02 to 1.23 at σ_3 = 100 kPa. The strength ratio can rise to SR = 1.53 for the sandwich specimen by using a sand layer with a thickness of 20 mm at σ_3 = 200 kPa. These results suggest that a sand layer can strengthen the soil-geotextile interaction. Regarding the effect of confining pressure, the results were somewhat scattered but clearly showed that the SR and SD values are increased by raising σ_3, which results from the behavior and strength of sand, depending highly on the confining pressure.

At $\sigma_3 \le 100$ kPa, no further shear-strength improvement was gained when a sand-layer thickness exceeded 10–15 mm. A similar range of sand thickness values (8–15 mm) was reported by Unnikrishnan et al. (2002) on the basis of their UU test results. At $\sigma_3 > 100$ kPa, an appreciable shear-strength improvement was still observed when the sand-layer thickness was increased from 15 to 20 mm. In contrast to the direct shear and pullout tests of previous studies (Abdi et al. 2009; Abdi and Arjomand 2011; Abdi and Zandieh 2014), a reduction in shear strength when providing sand-layer thicknesses over the optimal sand thickness was not observed in the test results in the present study. The optimal sand thickness, which depends on the types of soil and reinforcement, the size of the test apparatus, and the applied loading conditions, is probably associated with the failure mechanism of the interface shear band. Further investigation is required to understand the optimal thickness of the sand layer.

Comparing the effect of sand-layer thickness to the number of geotextile layers was also instructive. The test results showed that a sandwich specimen with a 10-mm sand layer and reinforced clay specimen with two geotextile layers had approximately the equivalent effect on the strength difference at σ_3 = 200 kPa, and a sandwich specimen with a 15-mm sand layer and reinforced clay specimen with two geotextile layers had a similar effect at σ_3 = 150 kPa.

Failure Envelope

Fig. 12 shows the failure envelopes of the unreinforced and reinforced clay specimens in the principal stress space. The stress at 20% strain was defined as failure deviatoric stress, as discussed previously in "Testing Program." As the number of reinforcing layers

Table 6. Summary of UU Test Results of Sandwich Specimens

Confining pressure (σ_3; kPa)	Unreinforced	Maximum deviatoric stress ($\sigma_{d,max}$; kPa)					
		Sand-layer thickness					
		0 mm[a]	5 mm	10 mm	15 mm	20 mm	Sand geotextile[b]
50	236.4	246.7	285.7	279.6	301.4	303.0	361.5
100	278.7	285.0	343.4	365.8	369.1	372.2	555.6
150	304.6	347.6	349.9	383.3	420.4	436.5	737.2
200	324.3	358.7	397.8	441.6	446.9	497.5	894.0

[a]The clay reinforced by a single layer of geotextile without a sand layer.
[b]Reinforced sand with a single layer of geotextile.

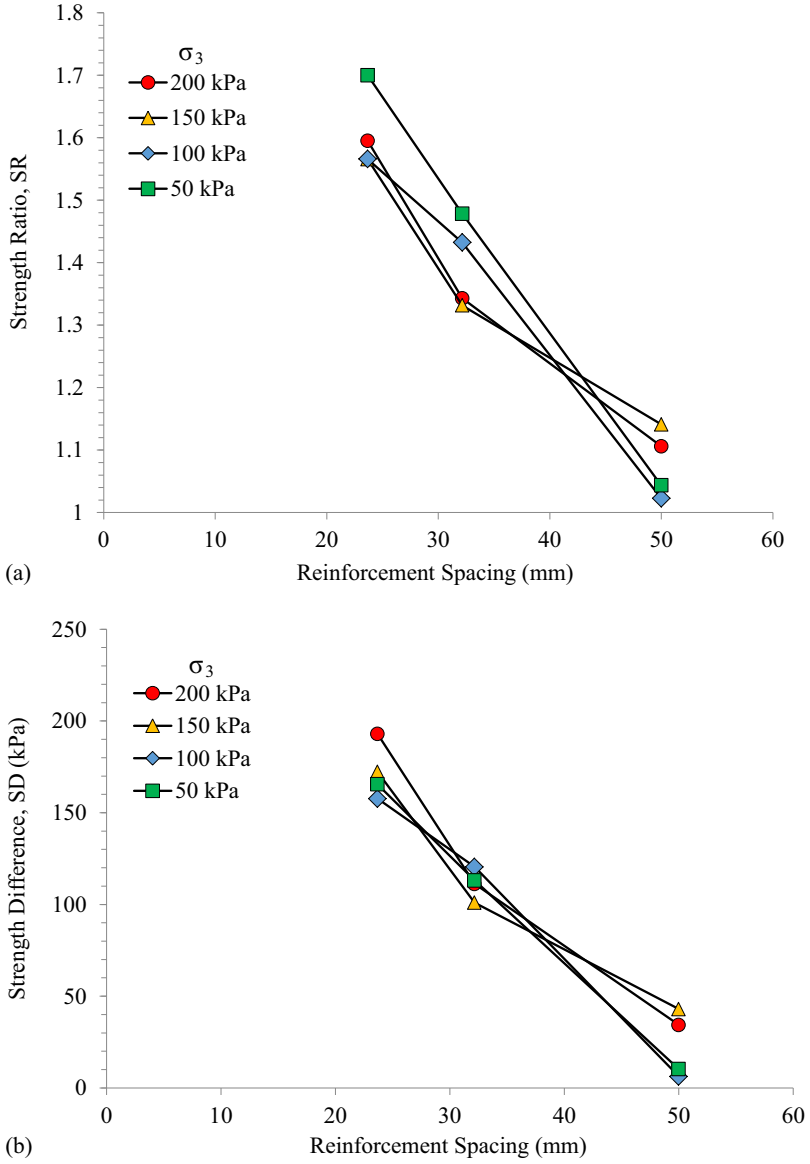

Fig. 10. Influence of reinforcement spacing on the shear-strength improvement for reinforced clay specimens: (a) SR; (b) SD

was increased, the failure envelopes of the reinforced clay specimens shifted upward. Because of weak clay-geotextile interaction under low confining pressure and large reinforcement spacing, the failure envelope of the reinforced clay with a single geotextile layer was close to that of the unreinforced clay. The failure envelopes of the reinforced clay with two and three geotextile layers appear to be parallel to that of the unreinforced clay. Parallel shifts in the failure envelopes of reinforced clay have also been reported by Noorzad and Mirmoradi (2010) and Al-Omari and Hamodi (1991). Except for the reinforced clay specimens with a single geotextile layer, the change in soil shear strength caused by reinforcement could be described by applying apparent cohesion theory, which was initially developed by Schlosser and Long (1974) on the basis of the test results of reinforced sand. The increase in reinforced soil shear strength was similar to that of the unreinforced soil improved by adding an amount of apparent cohesion. Applying apparent cohesion theory to the failure envelopes of the reinforced clay was limited by the conditions of high confining pressure or small reinforcement spacing, in which the clay-geotextile interaction was stronger and the mobilized geotextile tensile strength was higher.

Fig. 13 shows the effect of providing a thin layer of sand on the failure envelopes. In contrast to the results observed in the reinforced clay specimens, the slopes of the failure envelopes steepened as the thicknesses of the sand layers were increased, resulting in increases in the friction angles and slight decreases in the cohesion. Specifically, compared with the unreinforced clay, a reinforced clay specimen with a 20-mm sand-layer thickness exhibited an increase in friction angle from $\phi_u = 13.1°$ to 23.2° and a cohesion decrease from $c_u = 84.7$ to 79.3 kPa, which was a 77% increase in friction angle and only a 7% decrease in cohesion. A postexperiment inspection of dismantled clay specimens and deformed geotextile revealed that the observed shear-strength improvement could be attributed to improved soil-geotextile interaction at the sand-geotextile interface, as will be discussed in the next section.

Mobilized Reinforcement Tensile Strain

Fig. 14 presents the mobilized tensile strains resulting from variations in the number of geotextile layers and in the thickness of the

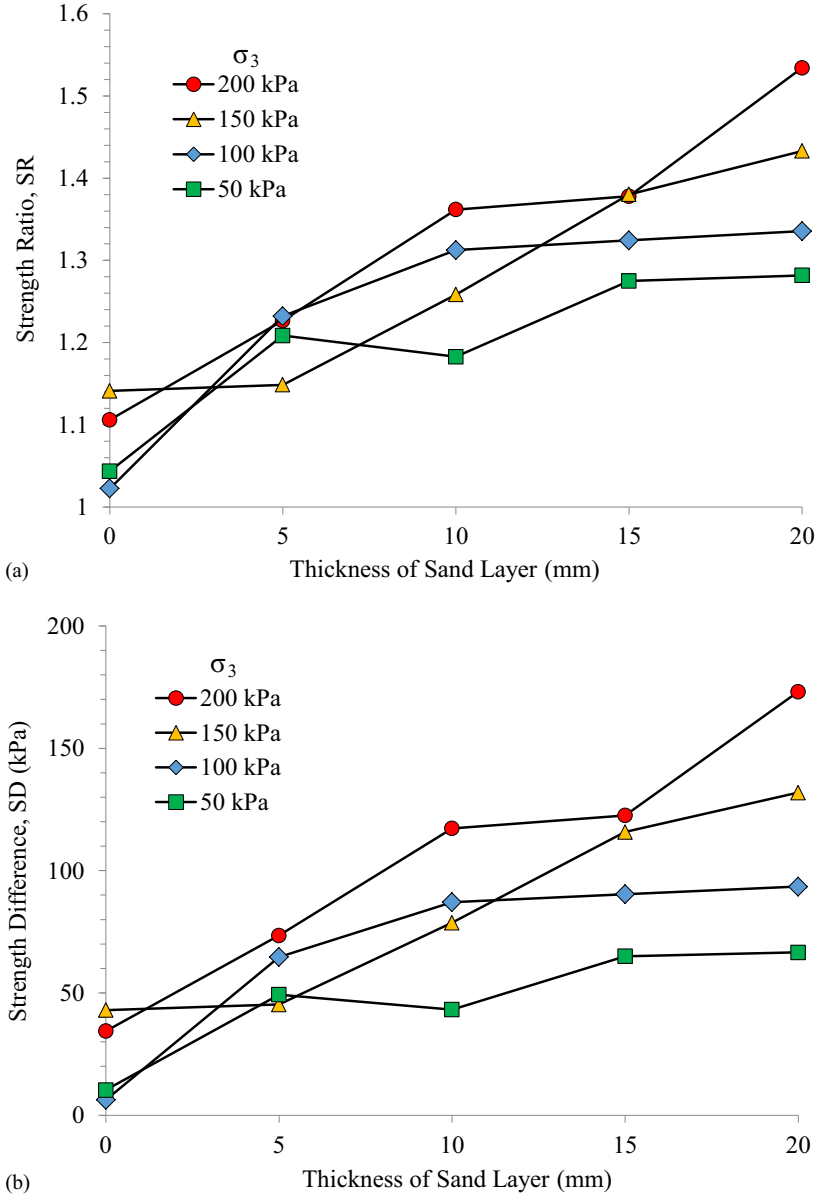

Fig. 11. Influence of sand layer thickness on the shear-strength improvement for sandwich specimens: (a) SR; (b) SD

sand layers. The mobilized reinforcement tensile strain was estimated from residual tensile strain, as discussed in "Technique for Measurement of Reinforcement Strain." The values of the mobilized tensile strain in a transverse (lower stiffness) direction are shown in Fig. 14 because the geotextile exhibited a larger deformation along this direction. The test results showed that the mobilized tensile strain increased with increases in the number of geotextile layers, thickness of the sand layer, and confining pressures, suggesting that these conditions enhanced the soil-reinforcement interaction, causing an increase in mobilized reinforcement tensile strain and force and, consequently, an increase in the shear strength of the reinforced clay.

In addition, as shown in Fig. 14(b), providing a thin layer of sand around the geotextile improved the mobilized tensile strain in the sandwich specimens. Compared with the mobilized tensile strains in the reinforced clay specimens with a single geotextile layer, the tensile strains in the sandwich specimens were mobilized substantially with an increase in sand-layer thickness, particularly under high confining pressure. Specifically, the mobilized tensile strain more than doubled (from 8.36 to 17.86%) as the thickness of the sand layer was increased from $t = 0$ to 20 mm at $\sigma_3 = 200$ kPa. This result confirmed that sand layers can enhance the soil-reinforcement interaction and further increase the shear strength of reinforced clay.

Fig. 15 shows the relationship between mobilized tensile strains in the geotextile and strength differences (i.e., net strength improvement by the effect of either reinforcements or sand layers). Fig. 15 also indicates values for the mobilized tensile force of the geotextile estimated by multiplying the mobilized tensile strain by the secant stiffness under axisymmetric loading measured from puncture-strength tests. As shown in Fig. 15, the mobilized tensile strain and force were strongly correlated with the strength difference. The data from both the reinforced clay and sandwich specimens fell into a unique linear relationship. This linear relationship demonstrated that the mobilized tensile strain and force directly contributed to the shear-strength improvement of

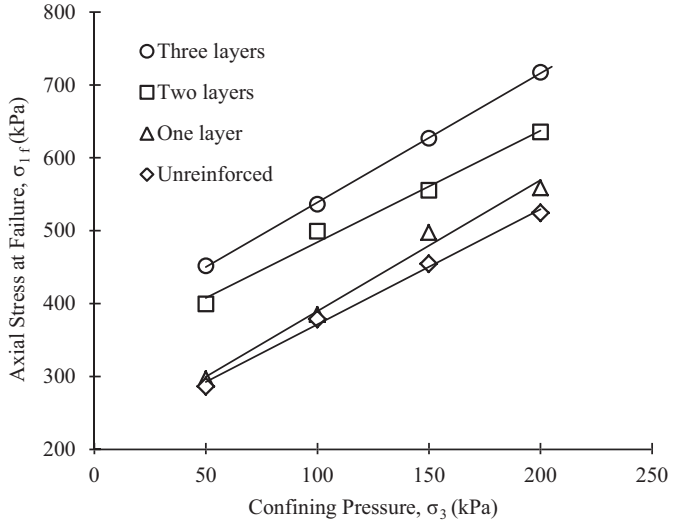

Fig. 12. Failure envelopes for unreinforced and reinforced clay

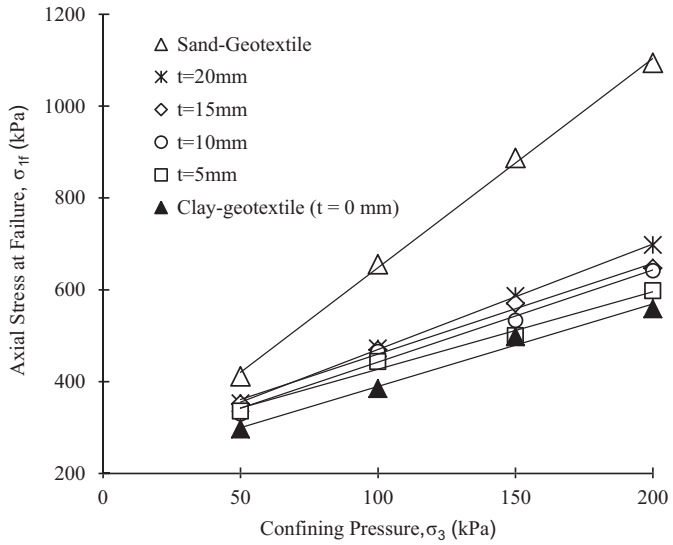

Fig. 13. Failure envelopes for sandwich specimens

the clay. Notably, no shear-strength improvement could be gained for a mobilized tensile strain of less than approximately 5% because of the nonlinear load-elongation responses of the geotextile. The reinforcement exhibited lower stiffness at a low strain level. As discussed in "Stress-Strain Behavior," the geotextile required sufficient deformation to mobilize its tensile force for improving the overall shear strength of the reinforced soil. Another possible explanation is that some tensile strains were mobilized during specimen preparation, before axial loading was applied.

Conclusions

A series of UU triaxial compression tests were performed to investigate the behavior and failure mechanisms of reinforced clay specimens with nonwoven geotextile and reinforced clay specimens with geotextile embedded in a thin layer of sand. The main goals of this work were to evaluate the effects of including nonwoven geotextile reinforcement layers and using the sandwich technique on the shear-strength improvement of clay, and to investigate the mobilization of reinforcement tensile strain/load within reinforced clay and their relationships with the mobilized shear strength of reinforced clay. The conclusions of this study can be summarized as follows:

- The reinforced clay specimens exhibited a ductile behavior that failed when bulging occurred between two adjacent reinforcement layers. The sandwich specimens failed because of the bulging of the clay and discontinuous deformation at the sand-clay interface.
- Both the reinforced clay and sandwich specimens enhanced the peak shear strength of the clay. The peak shear strength increased as the number of geotextile layers and the thickness of the sand layer increased.
- At low strain (up to 3–5% of the axial strain), the reinforced clay specimen exhibited a lower modulus compared with the unreinforced specimen. The mobilized shear strength of the sandwich specimens with thicker sand layer at low strain significantly increased and could exceed that of unreinforced clay.
- With a minimal 5-mm sand-cushion layer, the SR was improved from 1.04 to 1.20 and from 1.02 to 1.23 at $\sigma_3 = 50$ and 100 kPa, respectively. The SR rose to 1.53 for the sandwich specimen with a sand-layer thickness of 20 mm at $\sigma_3 =$ 200 kPa.
- Regarding the sandwich specimens, no further shear-strength improvement was gained when a sand-layer thickness exceeded the range of 10–15 mm at $\sigma_3 \le 100$ kPa, whereas an appreciable shear strength improvement was still observed when the sand-layer thickness was increased from 15 to 20 mm at $\sigma_3 > 100$ kPa. An optimal sand-layer thickness exceedance that led to a reduction in shear strength was not observed in test results for total sand-layer thicknesses tested up to 20 mm.
- The failure envelope of the reinforced clay with a single geotextile layer was close to that of the unreinforced clay because of weak clay-geotextile interaction under large reinforcement spacing. The failure envelopes of the reinforced clay with two and three geotextile layers appeared to be parallel to that of the unreinforced clay. The enhancement in shear strength could be explained by the increase in apparent cohesion. Regarding the sandwich specimens, the slopes of the failure envelopes steepened, causing an increase in the friction angles, as the thicknesses of the sand layers increased.
- The mobilized tensile strain increased with an increase in the number of geotextile layers, thickness of the sand layer, and confining pressures. This finding indicates a stronger soil-reinforcement interaction under these conditions. The mobilized tensile strain and force were strongly correlated with the strength difference in both the reinforced clay and sandwich specimens, demonstrating that mobilized tensile strain and force directly contribute to the shear-strength improvement of clay.

Finally, this investigation clearly demonstrated that small reinforcement spacing and thick sand layers can effectively strengthen the soil-geotextile interaction, thereby enhancing the shear strength of clay. Therefore, as a practical application, low-permeability and fine-grained soils could be used as backfill in reinforced structures by considering a proper drainage design and construction techniques that involve using permeable geotextile layers and providing layers of high-friction, coarse-grained soil around reinforcement.

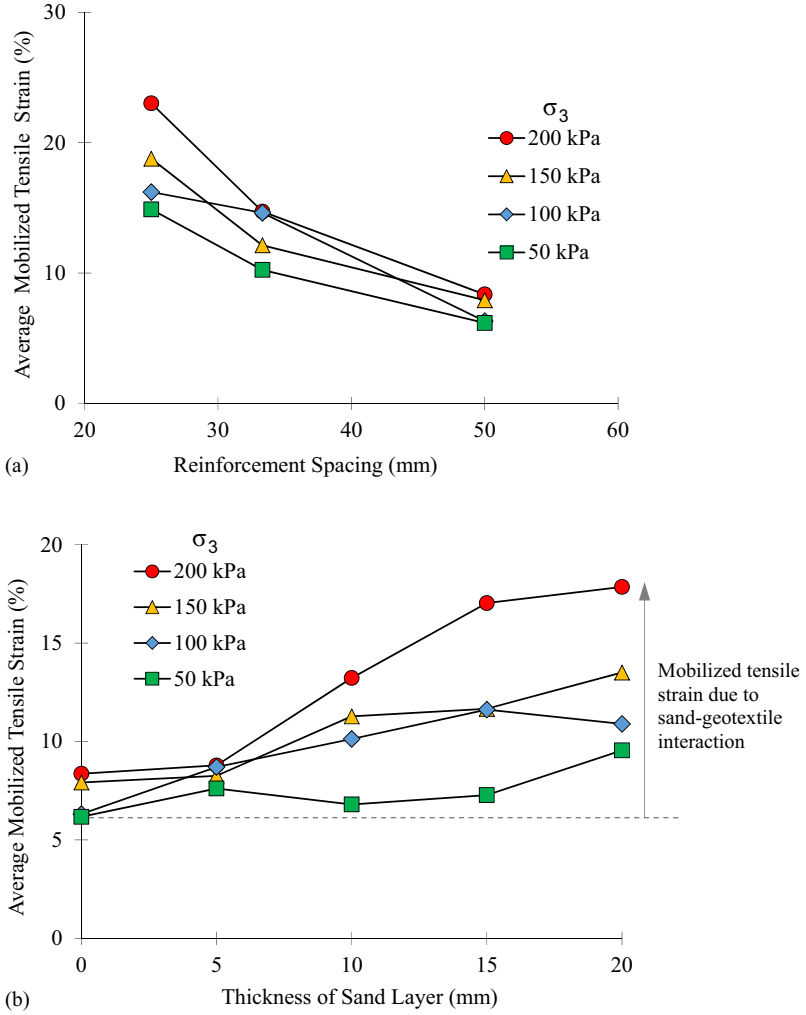

Fig. 14. Average mobilized tensile strain in transverse direction of geotextile: (a) reinforced clay specimens with different reinforcement layers; (b) sandwich specimens with different sand thicknesses

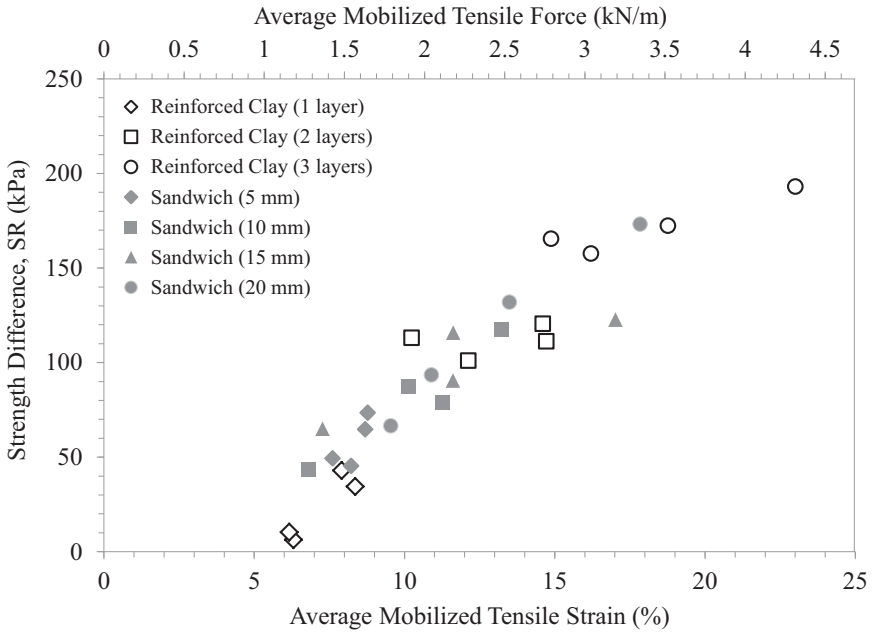

Fig. 15. Relationships between strength difference and average mobilized tensile strain for both reinforced clay and sandwich specimens

Acknowledgments

The financial support for this research was from the Ministry of Science and Technology of Taiwan under grant no. NSC102-2221-E-011-057-MY3. Financial support for the second and third authors during their graduate study was provided by the Taiwan Ministry of Education under a grant for the "Aim for the Top-Tier University Project." The authors gratefully acknowledge the financial supports.

Notation

The following symbols are used in this paper:

A = Skempton pore water pressure parameter (dimensionless);
a_0, a = initial and deformed length of geotextile under puncture strength test, respectively (m);
C_u, C_c = coefficient of uniformity and curvature, respectively;
c' = effective cohesion (Pa);
c_u = undrained cohesion (Pa);
D_{10}, D_{30}, D_{60} = diameter through which 10, 30, and 60% of the total soil mass is passing, respectively (m);
d, d' = diameter of the undeformed and deformed geotextile specimen, respectively (m);
G_s = specific gravity (dimensionless);
H = total height of specimens (m);
k_{sat} = saturated hydraulic conductivity (m/s);
LL = liquid limit (%);
P = measured puncture force (N);
PL = plastic limit (%);
r_p = radius of steel rod (m);
SD = strength difference (Pa);
SR = strength ratio (dimensionless);
T = tensile force per unit width of geotextile (N/m);
t = thickness of the sand layer (m);
y = vertical displacement of puncture rod (m);
β = angle between the deformed geotextile plane and initial horizontal position (degrees);
γ = unit weight (N/m^3);
$\gamma_{d,\min}$, $\gamma_{d,\max}$ = minimum and maximum dry unit weight, respectively (N/m^3);
ε = reinforcement mobilized tensile strain (dimensionless);
ε_a = axial strain (dimensionless);
ε_r = reinforcement residual tensile strain (dimensionless);
σ_d = deviatoric stress (Pa);
$\sigma_{d,\max}$ = maximum deviatoric stress (Pa);
$(\sigma_{d,\max})_{re}$, $(\sigma_{d,\max})_{un}$ = maximum deviatoric stress of reinforced and unreinforced specimens, respectively (Pa);
σ_{1f} = axial stress at failure (Pa);
σ_3 = confining pressure (Pa);
ϕ_u = undrained friction angle (degrees);
ϕ', ϕ_a' = effective friction angle of soil and soil-geotextile interface, respectively (degrees); and
ω_{opt} = optimum moisture content (%).

References

AASHTO. (2002). *Standard specifications for highway bridges*, 17th Ed., Washington, DC.
Abdi, M. R., and Arjomand, M. (2011). "Pullout tests conducted on clay reinforced with geogrid encapsulated in thin layers of sand." *Geotext. Geomem.*, 29(6), 588–595.
Abdi, M. R., Sadrnejad, A., and Arjomand, M. A. (2009). "Strength enhancement of clay by encapsulating geogrids in thin layers of sand." *Geotext. Geomem.*, 27(6), 447–455.
Abdi, M. R., and Zandieh, A. R. (2014). "Experimental and numerical analysis of large scale pull out tests conducted on clays reinforced with geogrids encapsulated with coarse material." *Geotext. Geomem.*, 42(5), 494–504.
Al-Omari, R. R., Al-Dobaissi, H. H., Nazhat, Y. N., and Al-Wadood, B. A. (1989). "Shear strength of geomesh reinforced clay." *Geotext. Geomem.*, 8(4), 325–336.
Al-Omari, R. R., and Hamodi, F. J. (1991). "Swelling resistant geogrid–A new approach for the treatment of expansive soils." *Geotext. Geomem.*, 10(4), 295–317.
ASTM. (2007). "Standard test method for particle-size analysis of soils." *ASTM D422*, West Conshohocken, PA.
ASTM. (2007a). "Standard test method for unconsolidated-undrained triaxial compression test on cohesive soils." *ASTM D2850*, West Conshohocken, PA.
ASTM. (2007b). "Standard test methods for water permeability of geotextiles by permittivity." *ASTM D4491*, West Conshohocken, PA.
ASTM. (2009). "Standard test method for the static puncture strength of geotextiles and geotextile-related products using a 50-mm probe." *ASTM D6241*, West Conshohocken, PA.
ASTM. (2011). "Standard test method for tensile properties of geotextiles by the wide-width strip method." *ASTM D4595*, West Conshohocken, PA.
ASTM. (2012). "Standard test methods for laboratory compaction characteristics of soil using standard effort." *ASTM D698*, Conshohocken, PA.
Berg, R., Christopher, B. R., and Samtani, N. (2009). "Design of mechanically stabilized earth walls and reinforced soil slopes." Vol.I and II. *Rep. No. FHWA-NHI-10-024*, National Highway Institute, Federal Highway Administration, Washington, DC.
Bergado, D. T., Youwai, S., Hai, C. N., and Voottipruex, P. (2001). "Interaction of nonwoven needle-punched geotextiles under axisymmetric loading conditions." *Geotext. Geomem.*, 19(5), 299–328.
Chen, J., and Yu, S. (2011). "Centrifugal and numerical modeling of a reinforced lime-stabilized soil embankment on soft clay with wick drains." *Int. J. Geomech.*, 10.1061/(ASCE)GM.1943-5622.0000045, 167–173.
Elias, V., Christopher, B. R., and Berg, R. (2001). "Mechanically stabilized earth walls and reinforced soil slopes design and construction guidelines." *Rep. No. FHWA-NHI-00-043*, National Highway Institute, Federal Highway Administration, Washington, DC.
Fabian, K. J., and Fourie, A. B. (1986). "Performance of geotextile-reinforced clay samples in undrained triaxial tests." *Geotext. Geomem.*, 4(1), 53–63.
Fourie, A. B., and Fabian, K. J. (1987). "Laboratory determination of clay geotextile interaction." *Geotext. Geomem.*, 6(4), 275–294.
Glendinning, S., Jones, C., and Pugh, R. (2005). "Reinforced soil using cohesive fill and electrokinetic geosynthetics." *Int. J. Geomech.*, 10.1061/(ASCE)1532-3641(2005)5:2(138), 138–146.
Indraratna, B., Satkunaseelan, K. S., and Rasul, M. G. (1991). "Laboratory properties of a soft marine clay reinforced with woven and nonwoven geotextiles." *Geotech. Testing J.*, 14(3), 288–295.
Ingold, T. S. (1983). "Reinforced clay subject to undrained traxial loading." *J. Geotech. Engrg.*, 10.1061/(ASCE)0733-9410(1983)109:5(738), 738–744.
Ingold, T. S., and Miller, K. S. (1982). "The performance of impermeable and permeable reinforcement in clay subject to undrained loading." *Q. J. Eng. Geol. Hydrogeol.*, 15(3), 201–208.
Ingold, T. S., and Miller, K. S. (1983). "Drained axi-symmetric loading of reinforced clay." *J. Geotech. Engrg.*, 10.1061/(ASCE)0733-9410(1983)109:7(883), 883–898.

Jamei, M., Villard, P., and Guiras, H. (2013). "Shear failure criterion based on experimental and modeling results for fiber-reinforced clay." *Int. J. Geomech.*, 10.1061/(ASCE)GM.1943-5622.0000258, 882–893.

Lin, C.-Y., and Yang, K.-H. (2014). "Experimental study on measures for improving the drainage efficiency of low-permeability and low-plasticity silt with nonwoven geotextile drains." *J. Chin. Inst. Civ. Hydraul. Eng.*, 26(2), 71–82 (in Chinese).

McGown, A., Andrawes, K. Z., Pradhan, S., and Khan, A. J. (1998). "Limit state design of geosynthetics reinforced soil structure." *Proc., Sixth Int. Conf. on Geosynthetics,* Vol. 1, Industrial Fabrics Association International, Roseville, MN, 143–178.

Mitchell, J. K. (1995). "Reinforced soil structures with poorly draining backfills. Part II: Case histories and applications." *Geosynth. Int.*, 2(1), 265–307.

NCMA (National Concrete Masonry Association). (2010). *Design manual for segmental retaining walls*, Herndon, VA.

Nguyen, M. D., Yang, K. H., Lee, S. H., Tsai, M. H., and Wu, C. S. (2013). "Behavior of nonwoven-geotextile-reinforced sand and mobilization of reinforcement strain under triaxial compression." *Geosynth. Int.*, 20(3), 207–225.

Noorzad, R., and Mirmoradi, S. H. (2010). "Laboratory evaluation of the behavior of a geotextile reinforced clay." *Geotext. Geomem.*, 28(4), 386–392.

Raisinghani, D. V., and Viswanadham, B. V. S. (2010). "Evaluation of permeability characteristics of a geosynthetic-reinforced soil through laboratory tests." *Geotext. Geomem.*, 28(6), 579–588.

Schlosser, F., and Long, N. T. (1974). "Recent results of French research on reinforced earth." *J. Constr. Div.*, 100(3), 223–237.

Sridharan, A., Murthy, B. R. S., and Revanasiddappa, K. (1991). "Technique for using fine-grained soil in reinforced earth." *J. Geotech. Eng.*, 10.1061/(ASCE)0733-9410(1991)117:8(1174), 1174–1190.

Taechakumthorn, C., and Rowe, R. (2012). "Performance of reinforced embankments on rate-sensitive soils under working conditions considering effect of reinforcement viscosity." *Int. J. Geomech.*, 10.1061/(ASCE)GM.1943-5622.0000094, 381–390.

Unnikrishnan, N., Rajagopal, K., and Krishnaswamy, N. R. (2002). "Behaviour of reinforced clay under monotonic and cyclic loading." *Geotext. Geomem.*, 20(2), 117–133.

Zornberg, J. G., and Mitchell, J. K. (1994). "Reinforced soil structures with poorly draining backfills. Part I: Reinforcement interactions and functions." *Geosynth. Int.*, 1(2), 103–148.